COMPUTATIONAL METHODS FOR DYNAMIC STABILITY AND CONTROL DERIVATIVES

Lawrence L. Green*
NASA Langley Research Center, Hampton, VA

Angela M. Spence**
Mississippi State University, Mississippi State, MS

Patrick C. Murphy***
NASA Langley Research Center, Hampton, VA

ABSTRACT

Force and moment measurements from an F-16XL during forced pitch oscillation tests result in dynamic stability derivatives, which are measured in combinations. Initial computational simulations of the motions and combined derivatives are attempted via a low-order, time-dependent panel method computational fluid dynamics code. The code dynamics are shown to be highly questionable for this application and the chosen configuration. However, three methods to computationally separate such combined dynamic stability derivatives are proposed. One of the separation techniques is demonstrated on the measured forced pitch oscillation data. Extensions of the separation techniques to yawing and rolling motions are discussed. In addition, the possibility of considering the angles of attack and sideslip state vector elements as distributed quantities, rather than point quantities, is introduced.

INTRODUCTION

Controlled aircraft flight requires the continuous and precise balance of aerodynamic, thrust, and inertial forces and moments over a variety of conditions. The forces and moments experienced by an aircraft during flight depend significantly on both the design details and the intended flight conditions of the vehicle.[1-5] Maneuvering forces and moments on an aircraft can be significantly different from the static forces and moments experienced during steady-state flight situations. Specifically, maneuvering forces and moments on an aircraft may exhibit nonlinear, time- and frequency-dependent behaviors, and damping and lag effects.[6] They may also involve the consideration of large angles of attack and sideslip, and moderate to massive flow separation.

Aircraft stability and control (S&C) derivatives quantify the changes in the aerodynamic forces or moments with respect to changes in the flow conditions or geometry of the vehicle; some S&C derivatives also quantify the changes in the aerodynamic forces or moments with respect to time. S&C derivatives are used to calculate, for example, the longitudinal short period, lateral pure roll, lateral-directional Dutch roll, spin behaviors, and handling qualities sensed by pilots for a given configuration.

A large base of knowledge regarding the S&C characteristics of past and present aircraft has been developed.[1-5, 7-8] However, aircraft designers, particularly those involved with the design of flight controls and flight control laws, are often called upon to provide S&C characteristics outside of the knowledge base in the design of advanced vehicles. They must account for the variation of the vehicle forces and moments for a variety of steady and maneuvering flight conditions. These specialists must provide S&C characteristics for proposed vehicles, as well as vehicle configurations that are simply modifications of existing aircraft. The needs to account for the variation in the forces and moments during flight and to predict S&C characteristics outside of the knowledge base, lead the aircraft designer to adopt, construct, and exercise a collection of "mathematical models." These models are used throughout the design and modification process to represent (at reduced cost compared to an actual flight vehicle) important features of the aircraft and its response to changing forces and moments throughout the flight envelope. Unfortunately, the term "model" is overused and ambiguously used in aircraft design; its definition varies from discipline to discipline and use of the term "model" may include anything from hardware (tested in a wind tunnel) to software

---

* Senior Research Scientist, Multidisciplinary Optimization Branch, M/S 159, Senior Member AIAA
** Engineering Co-op Student, Multidisciplinary Optimization Branch, M/S 159, Student Member AIAA
*** Senior Research Engineer, Dynamics and Control Branch, M/S 132, Associate Fellow AIAA

(computational simulation of vehicle dynamics) to mathematics (an assessment of which terms in the Navier-Stokes equations are relevant to a particular flight condition), or even combinations of the above, such as a piloted simulation of vehicle dynamics. The collection of "models" used by a designer most likely includes both static and dynamic versions, as well as one or more geometric, inertial, and aerodynamic representations to various fidelities of the vehicle.

Historically, aircraft static and dynamic S&C derivatives have been determined through wind tunnel or water tunnel tests, or with empirical estimates based on prior tests.[1-5, 7-9] Most of the wind tunnels and all of the water tunnels used for the determination of aircraft dynamic S&C derivatives operate at low free stream velocities and at low Reynolds numbers. These limitations restrict the range of flight conditions that can be adequately evaluated.

Many S&C testing facilities provide unique dynamic capabilities that are not typically available in the wind tunnels used for aircraft performance tests. Because of their dynamic capabilities, these S&C facilities may be expensive to build, operate, and/or maintain. The range of motions that can be performed in such facilities may be limited by the wind tunnel walls or by the test rig's kinematic and vibrational restrictions. Some facilities are not equipped with a "slip ring" capability and thus, cannot perform continuous rotary motions; instead they rely on oscillatory motions to provide brief periods of steady rotational motion. In addition, many conventional dynamic test facilities do not provide the capability to determine damping and cross derivatives individually; instead, these facilities can only provide measurements of combined derivatives.[6] The measurement of these combined quantities is not the preferred situation; it is simply a kinematic reality of the facilities available.

These derivative combinations are the in-phase and out-of-phase Fourier components. For example, the in-phase and out-of-phase components of the lift force coefficient are:

$$\bar{C}_{L_\alpha} = C_{L_\alpha} - k^2 C_{L_{\dot{q}}} \tag{1}$$

and

$$\bar{C}_{L_q} = C_{L_q} + C_{L_{\dot{\alpha}}} \tag{2}$$

where α is the vehicle angle of attack and q is pitch rate; both α and q are elements of the state vector. The reduced frequency, k, is defined later in this paper. The dot notation in Eqs. 1 and 2 refers to derivatives with respect to time.[6]

The states involved are for lateral motions are $(p, \dot{\beta})$, $(\dot{p}, \beta)$, $(r, \dot{\beta})$, and $(\dot{r}, \beta)$, where β is the vehicle angle of sideslip, and p and r are the vehicle roll and yaw angles, respectively. The mathematical basis for the existence of S&C quantities, including time derivatives of $\alpha, \beta, p, q,$ and r, is derived from a particular Taylor series expansion about a nominal flight condition. A considerable amount of work has been published recently suggesting that this choice of mathematical model may be incomplete for obtaining the damping and cross derivatives used to provide aircraft aerodynamic responses;[10-15] some alternative mathematical models[16-20] and improved testing techniques[21-28] have been proposed.

The difficulty of many experimental S&C facilities to adequately model the flight characteristics of today's aircraft over the entire flight envelope, the cost of developing better S&C testing facilities, and the recent advent of novel morphing aircraft configurations[29-31] all contribute to the difficulty of predicting S&C derivatives. Prior research efforts[30-47] using CFD to predict S&C derivatives have made some progress toward bridging the capability gap, but these efforts are very time consuming[32] and have failed to make a significant impact in the day to day business of S&C prediction. Because both CFD and experimental studies[11-12] have their unique disadvantages, aerospace companies spend millions of dollars fixing S&C problems discovered during certification flight tests or production use. The current situation for S&C prediction is similar to the situation seen before CFD methods were widely used to accurately predict aerodynamic performance.

As described more completely in a companion paper,[48] CFD offers several unique capabilities that complement experimental testing techniques for obtaining S&C derivatives. These unique capabilities of CFD include the ability to: 1) perform maneuvers without the flow/kinematic restrictions and support interference commonly associated with experimental S&C facilities, 2) easily simulate advanced S&C testing techniques, 3) compute exact S&C derivatives with uncertainty propagation bounds, and 4) alter the flow physics associated with a particular testing technique from those observed in a wind or water tunnel test in order to isolate effects. In addition, CFD can increase our understanding of the causes and types of separated flows affecting S&C prediction.

In theory, applying CFD to S&C prediction is not only feasible, but straight forward; one would grid the vehicle of interest and perform the required calculations. In practice, many issues must be addressed before CFD can accurately predict S&C derivatives, including: 1) the cultural differences in language usage, notation, and accuracy expectations that exist between the CFD and S&C communities, 2) the significant increase in computer resources

(execution time, memory, and disk space) required to address the aircraft S&C derivative needs[31-33] beyond the substantial resources already required for standard aircraft CFD performance calculations, 3) the need for uncertainty quantification of S&C derivatives used in flight simulations and multidisciplinary design efforts[49-53] and the further increase in computational resources associated with computing S&C predictions with uncertainty included,[49-51] and 4) the absence of a set of acceptable test cases that the CFD community must solve and the degree of accuracy required for CFD to become a credible alternative to wind and water tunnel testing.

This paper makes initial attempt to examine the computational simulation of combined (lumped) dynamic S&C derivatives. A widely distributed, low-order, time-dependent panel method CFD code was used to reduce the computational time involved, since the process itself was uncertain at the start of the research. The code offers the ability to compute time-dependent solutions for a variety of aircraft motions with modest computational time and memory requirements. The authors hoped that this code could be used for reasonable prediction of dynamic S&C characteristics within a conceptual or preliminary design environment. It was expected that trends of the amplitude and frequency effects observed in measured data could be simulated in the code, but that inability of the code to model vortical flow would be problematic in obtaining accurate solutions. However, as will be shown subsequently, the code inadequately predicted the frequency dependent behavior of dynamic S&C quantities for the test cases examined.

The paper also proposes three methods to computationally separate aircraft dynamic stability derivatives that are measured in combination during forced pitch oscillation dynamic motions. One of the separation techniques is demonstrated on measured forced pitch oscillation data. Because the computational simulation failed to correctly predict the expected frequency dependent dynamic S&C behavior, no separation technique was exercised on computed data and two of the separation methods could not be verified with the available measured data.

In addition, the possibility of considering the angles of attack and sideslip state vector elements as distributed quantities, rather than point quantities, is discussed. In the companion paper,[48] several computational techniques relevant to the calculation of dynamic S&C derivatives are demonstrated and the results of numerous grid resolution studies are presented.

TECHNICAL APPROACH

A particular combination of mathematical and computational techniques is used to predict aircraft dynamic S&C derivatives, including the computational separation of dynamic S&C derivatives measured in combinations. The mathematical techniques employed include the application of multivariable differential and integral calculus, the use of the Maple symbolic manipulation tool,[54] and the application of the ADIFOR automatic differentiation (AD) of FORTRAN tool[55-57] to a CFD code. These techniques enable the efficient calculation of first and second derivatives of the CFD code forces and moments with respect to a variety of code inputs. Table 1 illustrates the correlation of this paper's figures with the technical approach. Ideally, all of the cells inside the table (intersections of techniques and data sources) would have figure numbers associated with them. However, because the panel code failed to predict the correct dynamic behavior, and because not all the data required were measured, several combinations of techniques with various data sources remain to be illustrated.

Automatic Differentiation

Automatic differentiation[55-57] is a technique for augmenting computer programs with statements for the computation of derivatives. It relies on the fact that every function, no matter how complicated, is executed on a computer as a (potentially very long) sequence of elementary arithmetic operations and elementary functions evaluations (i.e., sine or cosine). By repeatedly applying the chain rule of differential calculus to the composition of those elementary operations, derivative information can be computed exactly and in a completely automated fashion.

Two approaches for computing derivatives with AD are the forward mode and the reverse mode. The forward mode applies the chain rule of differentiation to propagate, equation by equation, derivatives of intermediate variables with respect to the input variables. In contrast, the reverse (adjoint) mode propagates, in reverse through the program, the derivatives of the output variables with respect to the input variables. The forward mode is better suited to problems with fewer input variables than output variables, whereas the reverse mode is better suited to problems with fewer output variables than input variables. Many hybrids of the forward and reverse modes are possible, with complementary tradeoffs in required random access memory (RAM), disk space, and execution time.

The forward method of AD is implemented in ADIFOR, version 2.0D.[55, 56] The reverse mode and some second derivative capability are implemented in ADIFOR, version 3.0.[57] Both tools were developed jointly by the Center for Research on Parallel Computation at Rice University and the Mathematics and Computer Sciences Division at Argonne National Laboratory. Both tools have been used in this and prior

studies with CFD codes, but only results obtained by using ADIFOR 2.0D are shown in this paper. In general, to apply ADIFOR to a given FORTRAN 77 code, the user is only required to specify those program variable names that correspond to the independent and dependent variables of the target differentiation, and a starting point in the program from which the differentiation proceeds. The AD tool then determines the variables that require derivative computations, formulates the appropriate forward or reverse mode derivative expressions for these variables, and generates new FORTRAN 77 code for the computation of both the original simulation and the associated derivatives. The ADIFOR-generated code is compiled (with special libraries) and executed like the original code.

The forward mode of ADIFOR differentiation was used to compute the stability derivatives in this study because generally, only a few input, or independent, variables are identified for differentiation within a given code generation compared with the 12 output, or dependent, variables. The reverse mode of AD may be employed to calculate the S&C derivatives for morphing vehicles, as in References 28 and 29, where the potentially thousands of independent variables (perhaps, each surface grid point, along with the 30 or so flight condition and orientation variables) would greatly outnumber the 12 dependent variables.

Computational Separation of Dynamic S&C Derivatives Measured in Combination

Three different techniques to computationally separate dynamic derivatives, measured in combination, are proposed. The first method is simply an algebraic manipulation of certain equations from Reference 6; it is demonstrated on computed and measured data. The second method to computationally separate dynamic S&C derivatives employs AD to extract several derivatives, not typically measured during S&C tests, that are required to formulate sets of two algebraic equations in two unknowns for either longitudinal, lateral, or rolling forced oscillations. The two unknowns are then solved simultaneously at each time step throughout the computational simulation of a maneuver. The use of AD is only a choice of convenience; other techniques could be employed to obtain equivalent derivatives, at different computational costs. This method will be further developed in later sections. The third method to computationally separate dynamic derivatives is simply an algebraic variant of the first method; AD is used to obtain different sets of derivatives, which are then incorporated into other sets of equations that are solved simultaneously. Neither the of the latter two methods are demonstrated herein because : 1) not all the required data elements were available from the measured data, and 2) the computed data failed to exhibit the correct dynamic behavior.

Throughout the following discussion, three different kinds of data are required for use in each derivative separation calculation: 1) static force and moment data, 2) steady rotational rate data, and 3) unsteady forced oscillation data. The three types of data result from three different types of experiments or simulations. The primary focus here is on steady rotational and forced oscillation motions in pitch, but extensions to the roll and yaw motions are described. For forced oscillation motions, the aircraft model is installed on a sting. Two common types of sting are the straight and elbow varieties (see Figure 1). A straight sting extends rearward from the aft end of the model to, perhaps, a C-strut, which can be moved to make large changes to the angle of attack; these stings are typically used in aircraft performance testing. An elbow sting consists of a part that attaches to the upper or lower surface of the model, near the model's center of gravity, supported by a second part that extends rearward from the junction point to a C-strut. In the case of the elbow sting, the part attached to the model is articulated to allow for model motions distinct from the supporting member and the C-strut can be moved to provide large orientation changes. In either case, some drive mechanism is available to force the model through sinusoidal motions with an imposed amplitude and angular frequency. For the small-amplitude forced oscillation motions in pitch of an F-16XL fighter (see Figure 2) considered in Reference 6, an elbow sting was used and the amplitude of all oscillations, α_A, was set at 5 degrees. Various angular frequencies, ω, were imposed, ranging from about 3 to 18 radians per second. For such motions, the Euler pitch orientation angle, θ, is driven through a range of values of the form

$$\theta = \theta_0 + \omega\alpha_A sin(\omega t) \tag{3}$$

where θ_0 is the mean value of the oscillation. For the studies reported in Reference 6, θ_0 ranged from about 20 to 60 degrees; no frequency- or amplitude-dependent dynamic behavior was observed in studies for θ_0 below 20 degrees.

The angular pitch rate, q, is the derivative of θ with respect to time, i.e.,

$$q = \frac{d\theta}{dt} = \dot{\theta} = \omega\alpha_A cos(\omega t) \tag{4}$$

because the derivative of the constant θ_0 with respect to time is zero. The angular acceleration, $\dot{q}$, is the derivative of q with respect to time, i.e.,

$$\dot{q} = \frac{d\dot{\theta}}{dt} = \frac{d^2\theta}{dt^2} = -\omega^2 \alpha_A sin(\omega t) \tag{5}$$

The angle of attack is assumed to be given by

$$\alpha = \theta \tag{6}$$

The derivative of α with respect to time would thus be given by

$$\dot{\alpha} = \frac{d\alpha}{dt} = \dot{\theta} \tag{7}$$

In Reference 6, the forces and moments of the aircraft model are assumed to be functions of $\alpha, \dot{\alpha}, q, and\ \dot{q}$, as shown in this generic form

$$C_X = C_X(\alpha, \dot{\alpha}, q, \dot{q}) \tag{8}$$

where C_X is intended to mean any of the body or wind forces and moments. That is,

$$C_X = \left\{ C_N, C_A, C_{L,}, C_D, C_Y, C_M, C_n, C_\ell \right\} \tag{9}$$

where C_N is the normal force coefficient, C_A is the axial force coefficient, C_L is the lift force coefficient, C_D is the drag force coefficient, C_Y is the side force coefficient, C_M is the pitching moment coefficient, C_n is the yawing moment coefficient, and C_ℓ is the rolling moment coefficient, of which only the longitudinal coefficients ($C_N, C_L, and\ C_M$) are relevant for pitching motions. For forced oscillations in pitch, the increment in the lift coefficient with respect to its mean value is given by

$$\Delta C_L = \frac{\partial C_L}{\partial \alpha}\Delta\alpha + \frac{\ell}{V}\frac{\partial C_L}{\partial \dot{\alpha}}\dot{\alpha} + \frac{\ell}{V}\frac{\partial C_L}{\partial q}q + \left(\frac{\ell}{V}\right)^2 \frac{\partial C_L}{\partial \dot{q}}\dot{q} \tag{10}$$

where $\Delta\alpha = \theta$, and where $\frac{\ell}{V}$ is a ratio of the characteristic length, ℓ, and the free stream velocity, V. The in-phase and out-of-phase dynamic combined derivative terms, $\bar{C}_{L_\alpha}$ and $\bar{C}_{L_q}$, respectively, are given by (as in Eqs. 1 and 2)

$$\bar{C}_{L_\alpha} = C_{L_\alpha} - k^2 C_{L_{\dot{q}}} \tag{11}$$

$$\bar{C}_{L_q} = C_{L_q} + C_{L_{\dot{\alpha}}} \tag{12}$$

where the reduced frequency, *k*, in rad/sec is defined as

$$k = \frac{\omega \ell}{V} \tag{13}$$

and where $\frac{\ell}{V} = \frac{\bar{c}}{2V}$ for longitudinal motions and $\frac{\ell}{V} = \frac{b}{2V}$ for lateral motions; $\bar{c}$ is the mean aerodynamic chord length, and b is the model span. For this study, reduced frequencies were chosen to match those in Reference 6 (*k* = 0.081 to 0.397).

Sample in-phase and out-of-phase wind tunnel component data, $\bar{C}_{L_\alpha}$ and $\bar{C}_{L_q}$, from Reference 6 are shown in Figures 3 and 4, respectively, as functions of angle of attack in degrees for various values of *k*. The data are derived from integrals of the force and moment coefficient time histories by using the definition of $\Delta C_L = C_L(t) - C_{L_{mean}}$ and the formulas of Reference 6,

$$\bar{C}_{L_\alpha} = \frac{2}{\alpha_A n_c T}\int_0^{n_c T} \Delta C_L(t) sin(\omega t) dt \tag{14}$$

and

$$\bar{C}_{L_q} = \frac{2}{\alpha_A k n_c T}\int_0^{n_c T} \Delta C_L(t) cos(\omega t) dt \tag{15}$$

The combined derivatives shown in Figures 3 and 4 exhibit a strong frequency dependence for angles of attack between 20 and 60 degrees. For angles of attack in the range of 0 to 20 degrees, no such frequency dependence was observed; the data all collapsed to a common curve. Similar behavior is observed for the

lumped pitching moment and normal force coefficient derivative data shown in Figures 5 and 6.

The first method to computationally separate the individual derivatives of the terms in Eqs. 11 and 12 is based on the observation that if any two of the terms in either equation are available, then that equation can be rearranged to solve for the third term algebraically. For example, both $\bar{C}_{L_\alpha}$ and C_{L_α} (static lift curve slope) are available in Reference 6, but the steady rate C_{L_q} is not available there. Thus, Eq. 11 could be rearranged to solve for $C_{L_{\dot{q}}}$, but Eq. 12 cannot be solved for $C_{L_{\dot{\alpha}}}$ by using this technique since C_{L_q} is available directly from a forced oscillation experiment. The technique is illustrated in Figures 7, 8, and 9 for lift force, pitching moment, and normal force coefficients, respectively. In Figure 7, the dynamic derivative, $C_{L_{\dot{q}}}$, is obtained by rearranging the terms in Eq. 11 and using the known values of $\bar{C}_{L_\alpha}$ and C_{L_α}. In Figure 8, equations similar to Eq. 11, appropriate for the pitching moment, are used to solve for the dynamic derivative, $C_{M_{\dot{q}}}$. In Figure 9, the dynamic derivative, $C_{N_{\dot{q}}}$, is presented by a similar technique. No similar operations can be performed on the measured data to obtain derivatives with respect to $\dot{q}$ because the values with respect to q are not reported in Ref. 6.

One may wish to examine the time-dependent nature of the terms in each equation, or examine the interchangeability of computations and measurements within the combined derivatives to isolate effects. Thus, a more general approach for separating combined dynamic S&C is proposed. The second method to computationally separate the individual derivatives of the terms in Eqs. 11 and 12 follows from the above discussion. From application of the chain rule, and Eq. 8,

$$\begin{aligned}\frac{dC_X}{d\alpha_A} &= \frac{\partial C_X}{\partial \alpha}\frac{\partial \alpha}{\partial \alpha_A} + \frac{\partial C_X}{\partial \dot{\alpha}}\frac{\partial \dot{\alpha}}{\partial \alpha_A} \\ &\quad + \frac{\partial C_X}{\partial q}\frac{\partial q}{\partial \alpha_A} + \frac{\partial C_X}{\partial \dot{q}}\frac{\partial \dot{q}}{\partial \alpha_A} \\ \frac{dC_X}{d\omega} &= \frac{\partial C_X}{\partial \alpha}\frac{\partial \alpha}{\partial \omega} + \frac{\partial C_X}{\partial \dot{\alpha}}\frac{\partial \dot{\alpha}}{\partial \omega} \\ &\quad + \frac{\partial C_X}{\partial q}\frac{\partial q}{\partial \omega} + \frac{\partial C_X}{\partial \dot{q}}\frac{\partial \dot{q}}{\partial \omega}\end{aligned} \tag{16}$$

The above equations are solved simultaneously at each time step for $\frac{\partial C_X}{\partial \dot{\alpha}}$ *and* $\frac{\partial C_X}{\partial \dot{q}}$. An ADIFOR application is used to generate the $\frac{\partial C_X}{\partial \alpha_A}$ *and* $\frac{\partial C_X}{\partial \omega}$ terms. The $\frac{\partial C_X}{\partial \alpha}$ *and* $\frac{\partial C_X}{\partial q}$ terms, respectively, are obtained from the static, and steady rotational rate, force and moment data. As noted previously, it may be difficult to find tunnels in which derivatives with respect to q can be measured directly; in this case, some mix of computational and measured data may be required, or the method can be applied only to computational data. The remaining $\frac{\partial}{\partial \alpha_A}$ *and* $\frac{\partial}{\partial \omega}$ terms are derived from the analytic expressions given above as:

$$\begin{aligned}\frac{d\alpha}{d\alpha_A} &= \sin(\omega t) \\ \frac{d\alpha}{d\omega} &= t\alpha_A \cos(\omega t) \\ \frac{d\dot{\alpha}}{d\alpha_A} &= \omega\cos(\omega t) \\ \frac{\partial \dot{\alpha}}{\partial \omega} &= \alpha_A \cos(\omega t) - t\omega\alpha_A \sin(\omega t)\end{aligned} \tag{17}$$

and

$$\frac{\partial q}{\partial \alpha_A} = \omega cos(\omega t)$$
$$\frac{\partial q}{\partial \omega} = \alpha_A cos(\omega t) - t\omega\alpha_A sin(\omega t)$$
$$\frac{\partial \dot{q}}{\partial \alpha_A} = -\omega^2 sin(\omega t)$$
$$\frac{\partial \dot{q}}{\partial \omega} = -2\omega\alpha_A sin(\omega t) - t\omega^2\alpha_A cos(\omega t) \quad (18)$$

Although the Euler orientation angles, $\psi, \theta, and\ \phi$, have a specific definitions with respect to angular rotations in an Earth frame of reference and a specific order of application in flight dynamics, the reader is cautioned that inconsistent usage of these variables between the S&C and CFD disciplines can been a source of confusion. For example, the inputs to the PMARC code suggest that these angles can be specified independent of each other, ignoring the required ordering of the rotations (heading, pitch, and roll) in flight dynamics. Within the S&C community, local interpretations of the variables, within an aircraft maneuver, may take precedence over the conventional global notation with respect to the earth. Given these cautions, extensions to the above for roll and yaw are now presented. For rolling motions, (including the small angle assumption that $p = \dot{\phi}$),

$$\phi = \phi_0 + \phi_A sin(\omega t)$$
$$p = \dot{\phi} = \omega\phi_A cos(\omega t)$$
$$\dot{p} = \ddot{\phi} = -\omega^2\phi_A sin(\omega t)$$
$$\frac{\partial p}{\partial \phi_A} = \omega cos(\omega t)$$
$$\frac{\partial p}{\partial \omega} = \phi_A cos(\omega t) - t\omega\phi_A sin(\omega t)$$
$$\frac{\partial \dot{p}}{\partial \phi_A} = -\omega^2 sin(\omega t)$$
$$\frac{\partial \dot{p}}{\partial \omega} = -2\omega\phi_A sin(\omega t) - t\omega^2\phi_A cos(\omega t) \quad (19)$$

and assuming a similar development as above,

$$C_X = C_X(\beta, \dot{\beta}, p, \dot{p})\ and$$
$$\frac{dC_X}{d\phi_A} = \frac{\partial C_X}{\partial \beta}\frac{\partial \beta}{\partial \phi_A} + \frac{\partial C_X}{\partial \dot{\beta}}\frac{\partial \dot{\beta}}{\partial \phi_A} + \frac{\partial C_X}{\partial p}\frac{\partial p}{\partial \phi_A} + \frac{\partial C_X}{\partial \dot{p}}\frac{\partial \dot{p}}{\partial \phi_A}$$
$$\frac{dC_X}{d\omega} = \frac{\partial C_X}{\partial \beta}\frac{\partial \beta}{\partial \omega} + \frac{\partial C_X}{\partial \dot{\beta}}\frac{\partial \dot{\beta}}{\partial \omega} + \frac{\partial C_X}{\partial p}\frac{\partial p}{\partial \omega} + \frac{\partial C_X}{\partial \dot{p}}\frac{\partial \dot{p}}{\partial \omega} \quad (20)$$

solve the above equations simultaneously for $\frac{\partial C_X}{\partial \dot{\beta}}$ *and* $\frac{\partial C_X}{\partial \dot{p}}$.

For yawing motions, with small angle assumptions and ψ rotations about the body Z axis,

$$\psi = \psi_0 + \psi_A sin(\omega t)$$
$$r = \dot{\psi} = \omega\psi_A cos(\omega t)$$
$$\dot{r} = \ddot{\psi} = -\omega^2\psi_A sin(\omega t)$$
$$\frac{\partial r}{\partial \psi_A} = \omega cos(\omega t)$$
$$\frac{\partial r}{\partial \omega_Z} = \psi_A cos(\omega t) - t\omega\psi_A sin(\omega t)$$
$$\frac{\partial \dot{r}}{\partial \psi_A} = -\omega^2 sin(\omega t)$$
$$\frac{\partial \dot{r}}{\partial \omega_Z} = -2\omega\psi_A sin(\omega t) - t\omega^2\psi_A cos(\omega t) \quad (21)$$

and assuming a similar development as above,

$$C_X = C_X(\beta, \dot{\beta}, r, \dot{r}) \text{ and}$$

$$\frac{dC_X}{d\psi_A} = \frac{\partial C_X}{\partial \beta}\frac{\partial \beta}{\partial \psi_A} + \frac{\partial C_X}{\partial \dot{\beta}}\frac{\partial \dot{\beta}}{\partial \psi_A} + \frac{\partial C_X}{\partial r}\frac{\partial r}{\partial \psi_A} + \frac{\partial C_X}{\partial \dot{r}}\frac{\partial \dot{r}}{\partial \psi_A}$$

$$\frac{dC_X}{d\omega} = \frac{\partial C_X}{\partial \beta}\frac{\partial \beta}{\partial \omega} + \frac{\partial C_X}{\partial \dot{\beta}}\frac{\partial \dot{\beta}}{\partial \omega} + \frac{\partial C_X}{\partial r}\frac{\partial r}{\partial \omega} + \frac{\partial C_X}{\partial \dot{r}}\frac{\partial \dot{r}}{\partial \omega} \qquad (22)$$

solve the above equations simultaneously for $\frac{\partial C_X}{\partial \dot{\beta}}$ *and* $\frac{\partial C_X}{\partial \dot{r}}$.

The variable ω is used interchangeably in the above developments, although a specific ω would typically be associated with each rotation angle. The third method to computationally separate the individual pieces of the in-phase and out-of-phase dynamic derivative terms assumes the above relationships (Eqs. 4-7 and 17-18) for $\dot{\alpha}$ *and* $\dot{q}$ are known. The CFD code is then modified to allow these quantities to be time-dependent *inputs* to the code, even though these quantities would typically be considered time-dependent *outputs* of a computational simulation. The values of $\alpha, q,$ *and* θ are derived from the input values of $\dot{\alpha}$ *and* $\dot{q}$ at each time step. In this scenario, the CFD code can then be differentiated with respect to $\dot{\alpha}$ *and* $\dot{q}$ to directly compute the $\frac{\partial C_X}{\partial \dot{\alpha}}$ *and* $\frac{\partial C_X}{\partial \dot{q}}$ terms at each time step. If desired, these terms can then be assembled with the other required terms in Eq. 9 to form the lumped dynamic derivative quantities $\bar{C}_{L_\alpha}$ and $\bar{C}_{L_q}$ for comparison with measured data.

The Fourier transforms in Eqs. 14 and 15 can also be reversed to reconstruct approximations of measured data time histories of the forces and moments, by inputting the known lumped derivative coefficients $\bar{C}_{L_\alpha}$ and $\bar{C}_{L_q}$. This technique is illustrated in the results section of the paper.

The Computational Fluid Dynamics Code

The demonstrations presented herein employ a low-order panel method CFD code that was modified by applying AD to enable efficient computation of exact first and second force and moment derivatives with respect to a variety of code inputs. The panel method CFD code was chosen for its: 1) ability to simulate a wide variety of steady and time-dependent rotary and oscillatory aircraft motions commonly used experimentally to determine aircraft dynamic S&C derivatives, 2) fast execution and moderate computational resource requirements, and 3) amenability to processing by AD to compute derivatives that are exact to the formulation accuracy of the code solution. As discussed in the companion paper,[46] second derivatives were also computed in some cases to allow for input variable uncertainty propagation through the code to the output forces and moments and their first derivatives. As a result of the combination of the above mathematical techniques and the CFD choice, demonstrations of the computational separation of dynamic aircraft S&C derivatives could be rapidly performed for a variety of flow conditions. Sample results are presented for an F-16XL fighter configuration modeled with a coarse surface grid, shown in three-view in Figure 2, subject to the restrictions discussed in the companion paper[46] regarding the effects of surface resolution on the accuracy of the computed forces and moments and their derivatives.

The Panel Method Ames Research Center (PMARC) code,[58] version 14.10 potential flow solver is a FORTRAN 77 code that can compute surface pressures, forces, and moments of arbitrary shapes. The code assumes of inviscid, irrotational, and incompressible flow. Boundary layer and compressible corrections available but are not implemented in this study. PMARC can also compute solutions of unsteady, time-varying flow conditions for a variety of aircraft motions. The original PMARC code has been modified to allow for the input of a free stream Mach number, angle of attack, and angle of sideslip in degrees. The code was also modified to allow for processing with ADIFOR by replacing scratch I/O files access with common block access, and several lines of code must be inserted into the program to identify independent and dependent variables of differentiation.

The input file to the program uses a set of grid points describing the shape of the geometry as a set of panels. In this study, both the right and left halves of a modified F-16XL configuration are modeled in the PMARC input file. The colors/gray-scale in Figure 2 reflect different surface patches in the PMARC geometry input file. The surface resolution, consisting of 984 surface points and 566 surface panels, is moderately coarse by CFD standards, yet the vehicle is

still clearly identifiable. The grid files are available to allow for calculations to be performed with higher surface resolutions (see discussion of Grid Resolution Studies in Reference 46). PMARC allows the user to describe only half the aircraft and mirror the solution in the *x*-*z* plane. However, this technique does not capture the effects of a nonzero angle of sideslip that are of interest later in this study. The input file also specifies the flight condition, certain algorithmic parameters, and the user-defined position of the reference center about which all moments are summed. The forces and moments are also nondimensionalized with a user-specified reference area, length of the mean aerodynamic chord, and wingspan. All runs were performed with the assumption of incompressible flow or low-speed flight conditions.

The PMARC code includes a wide variety of possible aircraft motions: 1) straight translation with imposed angles of attack (α) and sideslip (β), 2) pure rotary motions about the three body axes described of constant rotational rates ($p, q, and\ r$), and 3) planar oscillatory motions in both translation and rotation about each of three body axes, each described by an amplitude and frequency, and 4) coning motions used within advanced experimental S&C facilities. In contrast to the limitations of some experimental facilities, these coning motions can be simulated within PMARC with either continuous (i.e., a "slip ring") or limited roll motion capability (oscillatory test motion).

In addition, the authors use two other capabilities of the CFD code that are not generally available to S&C experimentalists. These capabilities are: the choice of using either rigid or flexible wakes, and the ability to somewhat arbitrarily change the time stepping characteristics of the solution. Although flexible wakes are preferred because they better model the flow physics involved, the flexible wakes are less robust during PMARC execution than are the rigid wakes for some of the motions of interest. Either flexible or rigid wakes are currently attached to the wing trailing edges and the upper vertical tail trailing edge. The time stepping characteristics of a given solution can be made to match the data sampling rate of a particular S&C facility, or input to provide higher or lower data sampling rates. A caveat of this technique is that the size of the shed wake panels in the PMARC solution is proportional to the chosen time step, which alters the flow physics to some extent if sufficiently small time steps are not used.

Distributed Angles of Attack and Sideslip

A fundamental issue involving kinematics, dynamics, and aerodynamics arises during forced oscillation maneuvers, independent of the choice of sting type (see Fig. 1). Using an elbow sting merely reduces the consequences of the issue. For the elbow sting used in Reference 6, the model undergoes rigid body rotation about a rotation center, coinciding with the balance moment center. Because of the rigid body motion, every point within the model moves in a circular arc path centered at the rotation center. The tangential velocity of each point in the body is different, depending on the point's distance from rotation center. As a result of this rigid body motion, a dynamic angle of attack may be considered to be imposed at each point of the body. The assumption that $\alpha = \theta$, during the forced oscillation motions, is really only true at the rotation center, or for infinitesimally small rotation rates. In reality, each point *P* in the body experiences an angle of attack imposed by the rigid body rotation, the effects of which are present in the integrated forces and moments of the vehicle . The components of this imposed angle of attack are increments to the free stream velocity and are given by

$$
\begin{aligned}
&(X_P, Z_P) = location\ of\ interest\ in\ body \\
&(X_{cr}, Z_{cr}) = model\ center\ of\ rotation\ location \\
&r = \sqrt{\left(X_P - X_{cr}\right)^2 + \left(Z_P - Z_{cr}\right)^2} \\
&X_P = X_{cr} + r\cos(\theta) \\
&Z_P = Z_{cr} + r\sin(\theta) \\
&V_X = \frac{dX_P}{dt} = -r\sin(\theta)\dot{\theta} \\
&V_Z = \frac{dZ_P}{dt} = r\cos(\theta)\dot{\theta}
\end{aligned}
\qquad (23)
$$

It would be convenient if this increment in angle of attack imposed by rigid body rotation could be thought of as an increment to that of the free stream, but it apparently does not lend itself well to this interpretation. If one considers a distributed angle of attack variable within the above equations (16), (20), or 22), which are to be solved simultaneously, additional terms will arise from Eq. 23 (and similar developments for sideslip, not shown). Because of the products of sines and cosines with the harmonic function, $\dot{\theta}$, these additional terms have strongly nonlinear and frequency-dependent effects, as well as dependence upon the physical scale of the vehicle under consideration. The terms arise from both geometric and kinematic considerations of the model

being tested. Examination of this effect is underway and may be the subject of continued future research.

RESULTS

Figures 10 and 11 show measured and computed in-phase and out-of-phase lumped lift force coefficient derivative data, $\bar{C}_{L_\alpha}$ and $\bar{C}_{L_q}$, for the two extreme values of *k* examined in Reference 6. The PMARC-computed data essentially captures an average effect of the dynamics, but fails to capture any of the frequency dependence observed in the measured data. Similar behavior is observed in the measured and computed in-phase and out-of-phase lumped pitching moment coefficient derivative data, not shown in this paper. For normal force coefficient derivative data, the discrepancy between measured and computed data is even worse, as shown in Figure 12 for $\bar{C}_{N_\alpha}$. The computed data fails to capture even the average behavior of the measured data. These results significantly undermine the proposed use of the PMARC code for the prediction and analysis of dynamic S&C derivatives.

PMARC may have failed to capture the measured dynamics because the code is unable to model either vertical or viscous flow phenomena. This guess cannot be verified without resorting to Euler and Navier-Stokes codes; even then, no direct comparison with PMARC's results can be made. Most Euler / Navier-Stokes codes cannot be easily run without vorticity effects included (whereas viscous effects can usually be easily turned off with Navier-Stokes codes).

Further proof of the suspect dynamics within PMARC can be seen in the four sets of data presented in Figure 13, which is similar to Figure 14 in Reference 6. In Figure 13, an approximation to the measured static normal force coefficient data curve (upper line segments and ellipses) has been reconstructed from several discrete forced oscillation maneuvers at $k = 0.081$ (dashed lines) and $k = 0.397$ (solid lines). The Fourier coefficients in Ref. 6 were used to determine the approximate time histories of the forces and moments. The reconstructed measured data sets (upper ellipses, green and black) are compared with computed results (lower ellipses, red and blue, including start-up transients) obtained from the PMARC time histories for the same maneuvers. In addition to the PMARC computation failing to match the levels of C_N at a given angle of attack, primarily because of the coarse grid resolution used as discussed in the companion paper[48], the PMARC computation fails to match the observed frequency dependent behavior of the lumped dynamic derivatives.[6]

In all cases of Figure 13, the lengths of the semi-major axis of the ellipses are proportional to the amplitudes of the oscillation. The PMARC results show similar sized ellipses for all angles of attack; the length of the semi-minor axis of the PMARC ellipses is proportional to *k* (red ellipses with k=0.397 have larger semi-minor axis than blue ellipse with k=0.081). In contrast, ellipses occur within the reconstructed measured data only for angles of attack above 20 degrees, as reported in Reference 6; the ellipses collapse to line segments for angles of attack below 20 degrees, indicating a lack of unsteady behavior for these cases. Moreover, the inclination of the reconstructed ellipses varies with angle of attack, and the length of the semi-minor is inversely proportional to the value of k (green ellipses with k=0.081 have larger semi-minor axis than black ellipses with k=0.397), where ellipses exist at all. The S&C community would typically associate a damping or lag behavior with the ordinate displacement of the ellipse curves in Figure 13 from their respective centroids. However, by either means of describing the curves in Figure 13, the dynamic behavior predicted by the PMARC code is clearly different from the behavior of the measured data for the cases examined. Further research must be conducted with the code to determine if it can be validated for use with more benign flow conditions for dynamic S&C derivative applications.

CONCLUSIONS

Clearly, the PMARC low-order panel method code to fails to predict basic and essential features of the measured dynamic data for the F-16XL configuration. This failure significant limits the proposed code usage within conceptual and preliminary design efforts and simultaneously renders two of the proposed separation techniques without means for immediate validation. The PMARC studies should be repeated with other configurations in an attempt to eliminate the effects of vortical and viscous flows. In addition, the studies should be repeated with Euler and Navier-Stokes codes to isolate the vortical and viscous effects within the F-16XL dynamic maneuvers.

This paper also proposed three techniques to computationally separate dynamic aircraft stability and control derivatives measured in combination. One of the techniques was used to obtain new dynamic derivative information for this vehicle. The other two separation techniques could not be demonstrated in this paper because of: 1) a lack of a required data element from the measured data set, and 2) the inability of the panel method code to adequately simulate the observed lumped dynamic derivative behaviors. The notion of distributed angles of attack and sideslip were introduced. It is recommended that further study of

this concept be conducted. Finally, the capabilities demonstrated herein could be implemented in any CFD code, or at any grid resolution within a given code to increase the level of flow physics represented in the calculations and the user's confidence in the predicted results.

REFERENCES

1. Nicolai, Leland M., *Fundamentals of Aircraft Design*, METS, Inc. Xenia, Ohio, 1975.
2. Roskam, Jan, *Airplane Flight Dynamics and Automatic Flight Controls, Parts I and II*, DARcorporation, Lawrence, Kansas, 2001.
3. Roskam, Jan, *Airplane Design, Part VII: Determination of Stability, Control, and Performance Characteristics: FAR and Military Requirements*, DARcorporation, Lawrence, Kansas, 2002.
4. Nelson, Robert C., *Flight Stability and Automatic Control (Second Edition)*, McGraw Hill International Editions Aerospace Science & Technology Series, New York, New York, 1998.
5. Etkin, B.: Dynamics of Atmospheric Flight, John Wiley & Sons, Inc., New York, 1972.
6. Klein, V., Murphy, P. C., Curry, T. J., and Brandon, J. M., "Analysis of Wind Tunnel Longitudinal Static and Oscillatory Data of the F-16XL Aircraft," NASA/TM-97-206276.
7. Roskam, Jan, *Advanced Aircraft Analysis (Software Package and Documentation)*, DARcorporation, Lawrence, Kansas, 2001.
8. McDonnell Douglas Astronautics Company, St. Louis Division, *The USAF Stability and Control DATCOM, Volume I, Users Manual*, McDonnell Douglas Astronautics Company, St. Louis Division, St. Louis, Missouri, 1979.
9. Lan, Edward C., "VORSTAB - A Computer Program for Calculating Lateral-Directional Stability Derivatives with Vortex Flow Effect," NASA Contractor Report 172501, January 1987.
10. Tavoularis, S., "Equivalence Between Sideslip and Roll In Wind-Tunnel Model Testing," AIAA J. Aircraft, Vol. 36, No. 5, pages 895-896, May, 1999.
11. Brandon, J.M., and J.V. Foster: Recent Dynamic Measurements and Considerations for Aerodynamic Modeling of Fighter Airplane Configurations, AIAA 98-4447, August 1998.
12. Klein, V., and Noderer, K.D.: Modeling of Aircraft Unsteady Aerodynamic Characteristics", Part I – Postulated Models, NASA TM 109120, May, 1994; Part 2 – Parameters Estimated From Wind Tunnel Data, NASA TM 110161, April 1995; Part 3 – Parameters Estimated From Flight Data, NASA TM 110259, May 1996.
13. Greenwell, D.J.: Difficulties in the Application of Stability Derivatives to the Maneuvering Aerodynamics of Combat Aircraft, ICAS 98-3.9.2, September 1998, Melbourne, Australia.
14. Goman, M.G., and Khrabrov, A.N., State-Space Representation of Aerodynamic Characteristics of an Aircraft at High Angles of Attack, Journal of Aircraft, Vol.31, No.5, September-October, 1994, pp. 1109-1115.
15. Ogburn, M.E., Nguyen, L.T., and Hoffler, K.D.: Modeling of Large-Amplitude High Angle-of-Attack Maneuvers, AIAA 88-4357, Atmospheric Flight Mechanics Conference, August 1988.
16. Klein, V., Batterson, J.G., Murphy, P.C.: Determination of Airplane Model Structure from Flight Data by Using Modified Stepwise Regression, NASA TP 1916, 1981.
17. Jones, R.T.: Transient Effects of the Wing Wake on the Horizontal Tail, NACA TN No. 771, 1940.
18. Buttrill, Carey S: Aeroservoelastic Simulation of an Active Flexible Wing Wind Tunnel Model, NASA TP 3510, 1996.
19. Tobak and Schiff: On the Formulation of the Aerodynamic Characteristics in Aircraft Dynamics, NASA TR R-456, 1976.
20. Goman, M. and Khrabrov, A: State-Space Representation of Aerodynamic Characteristics of an Aircraft at High Angles of Attack. Journal of Aircraft, Vol.31, No.5, 1994, pp. 1109-1115.
21. Khrabrov, A., et.al.: Using of Oscillatory Conning Experimental Rig for Separation of Rotary and Unsteady Aerodynamic Derivatives, 18th ICIASF, Toulouse, France, June 1999.
22. Goman, M.G., Greenwell, D. I., Khrabrov, A. N.: The Characteristic Time Constant Approach for Mathematical Modeling of High Angle of Attack Aerodynamics, ICAS 2000 Congress.
23. Jenkins, J. E., Myatt: Body-Axis Rolling Motion Critical States of a 65-Degree Delta Wing, J of Aircraft, March-April, 1996.
24. Klein, V. and Murphy, P.C.: Estimation of Aircraft Nonlinear Unsteady Parameters from Wind Tunnel Data, NASA/TM-1998-208969, December 1998.
25. Schroeder, M.R.: Synthesis of Low-Peak-Factor Signals and Binary Sequences with Low Autocorrelation, IEEE Transactions on Information Theory, January 1970, pp.85-89.
26. Murphy, P. C., Klein, V.: Estimation of Aircraft Unsteady Aerodynamic Parameters From Dynamic Wind Tunnel Testing, AIAA 2001-4016, August 2001.

27. Kramer, Brian R.: Experimental Evaluation of Superposition Techniques Applied to Dynamic Aerodynamics. AIAA 2002-0700, January 14-17, 2002.
28. Eidetics Corporation: Aircraft Dynamics: Nonlinear Math Modeling. Annual Report June 2002, Contract NAS1-01091.
29. Dorsett, K. M., and Mehl, D. R., “Innovative Control Effectors (ICE),” Wright Laboratory Report, WL-TR-96-3043, Jan. 1996.
30. Raney, D. L., Montgomery, R. C., and Green, L. L., and Park, M. A., "Flight Control Using Distributed Shape-Change Effector Arrays," AIAA 2000-1560, April 2000.
31. Park, M., Green, L., Montgomery, R., and Raney, D., “Determination of Stability and Control Derivatives Using Computational Fluid Dynamics and Automatic Differentiation,” AIAA paper 99-3136, June 1999.
32. Park, Michael A. and Green, Lawrence L., "Steady-State Computation of Constant Rotational Rate Dynamic Stability Derivatives, AIAA 200-4321, August 2000.
33. Park, Michael A., *Determination of Static and Dynamic Stability and Control Derivatives With Computational Fluid Dynamics and Automatic Differentiation*, Master Thesis, The George Washington University, August 2000.
34. Limache, A. C., and Cliff, E. M., “Aerodynamic Sensitivity Theory for Rotary Stability Derivatives,” AIAA Paper 98-4313, Aug. 1998.
35. Gainer, Thomas G., "A Discrete-Vortex Method for Studying the Wing Rock of Delta Wings," NASA/TP-2002-211965, December 2002.
36. Melville, Reid, "Aeroelastic Instability of Tactical Aircraft in Nonlinear Flow Regeims," AIAA 2002-2970, June, 2002.
37. Jouannet, C. and Krus, P., "Lift Coefficient Predictions for Delta Wing Under Pitching Motions," AIAA 2002-2969, June 2002.
38. Kay, Jacob, "Acquiring and Modeling Unsteady Aerodynaimc Characteristics," AIAA 2000-3907, August 2000.
39. Katz, Joseph, and Schiff, Lewis B., "Modeling Aerodynamic Responses to Aircraft Maneuvers-A numerical Validation," AIAA J. Aircraft, Vol. 23, No. 1, January 1986.
40. van Dam, C. P., DalBello, T., and Chao, D. D., "Prediction of Flows About Forebodies at High-Angle-of-Attack Dynamic Conditions," Final Report of NASA Langley Research Center Grant NAG-1-2006, May 2000.
41. Youngren, H. H., Bouchard, E. E., Coopersmith, R. M., and Miranda, L. R., “Comparison of Panel Method Formulations and its Influence on the Development of QUADPAN, an Advanced Low Order Method,” AIAA Paper 83-1827, July 1983.
42. Miranda, L. R., Elliott, R. D., and Baker, W. M., “A Generalized Vortex Lattice Method of Subsonic and Supersonic Flow Applications,” NASA CR-2865, Dec. 1977.
43. Simon, J. M., “Dynamic Derivative Data for High-Angle-of-Attack Simulation,” AIAA paper 92-4355, Aug. 1992.
44. Blake, W. B., Dixon, C. J., and Adler, C. O., “Development of a High-Angle-of-Attack Stability and Control Prediction Code,” AIAA Paper 92-4354, Aug. 1992.
45. Ahn, T., Kim, C., Rho, O. H., and Kim, H.-J., "Dynamic Stall Control Using Aerodynamic Sensitivity Analysis," AIAA 2001-0255, January 2001.
46. 1988 Report to the Aerospace Profession XXXIII, Thirty-Third Symposium Proceedings, September 1989.
47. Albright, A. E., Dixon, C. J., Hegedus, M. C., “Modification and Validation of Conceptual Design Aerodynamic Prediction Method HASC95 With VTXCHN,” NASA CR-4712, Mar. 1996.
48. Green, Lawrence L., and Spence, A. M.: Applications of Computational Methods for Dynamic Stability and Control Derivatives. AIAA 2004-0377, January 5-8, 2004.
49. Putko, M. M., Taylor, III, A. C., Newman, P. A., and Green, L. L., “Approach for Input Uncertainty Propagation and Robust Design in CFD Using Sensitivity Derivatives,” Journal of Fluids Engineering, published by the Society of Mechanical Engineers, Vol. 124, No. 1, March 2002, pp. 60-69 (see also.AIAA Paper 2001-2528, June 2001).
50. Hosder, S., Grossman, B., Haftka, R. T., Mason, W. H., and Watson, L. T., Observations on CFD Simulation Uncertainties, AIAA 2002-5531, September 2002.
51. Green, L., Lin, H.-Z., and Khalessi, M., "Probabilistic Methods for Uncertainty Propagation Applied to Aircraft Design,", AIAA Paper 2002-3140, June 2002.
52. Hemsch, M., "Statistical Analysis of CFD Solutions from the Drag Prediction Workshop," AIAA 2002-0842, January 2002.
53. Eca, L., Vaz, G. B., and Falco de Campos, A. C., "Verification Study of Low and Higher-Order Potential Based Panel Methods for 2D Foils," AIAA 2002-3112, June 2002.

54. K. C. Chan, A. Daz, and E. Kaltofen, “A distributed approach to problem solving in Maple,” In R. J. Lopez, editor, Maple V: Mathematics and its Application, Proceedings of the Maple Summer Workshop and Symposium (MSWS'94), pages 13-21, Boston, 1994. Birkhauser.

55. Bischof, C., Carle, A., Corliss, G., Griewank, A., and Hovland, P., “ADIFOR—Generating Derivative Codes from Fortran Programs,” *Scientific Programming*, No. 1, 1992, pp. 1–29.

56. Bischof, C., Carle, A., Khademi, P., and Mauer, A., “Automatic Differentiation of FORTRAN,” *IEEE Computational Science & Engineering*, Fall 1996.

57. Carle, A. and Fagan, M., “Overview of Adifor 3.0,” Department of Computational and Applied Mathematics, Rice University, CAAM-TR 00-02, Jan. 2000.

58. Ashby, Dale L., Dudley, Michael R., Iguchi, Steve K., Browne, Lindsey, and Katz, Joseph, "Potential Flow Theory and Operation Guide for the Panel Code PMARC," NASA TM 102851, January 1991. (Unofficially revised in 1999 for PMARC version 14).

Table 1 Correlation of paper figures with technical approach.

Technique	Measured Data	PMARC Data	Navier-Stokes Data
Lumped Dynamic Derivatives	Figures 3-6	Figure 10-12	Subject Of Future Research
Separation Technique 1	Figures 7-9	Not Attempted Due To Figures 10-13	Subject Of Future Research
Separation Technique 2	Insufficient Data	Not Attempted Due To Figures 10-13	Subject Of Future Research
Separation Technique 3	Insufficient Data	Not Attempted Due To Figures 10-13	Subject Of Future Research
Extension of separation techniques to include distributed angle of attack and sideslip effects	Insufficient Data	Not Attempted Due To Figures 10-13	Subject Of Future Research

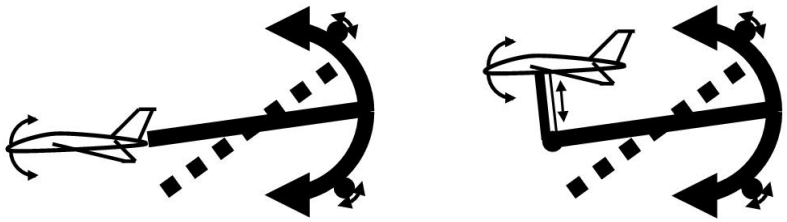

Figure 1. Schematic of straight and elbow test stings.

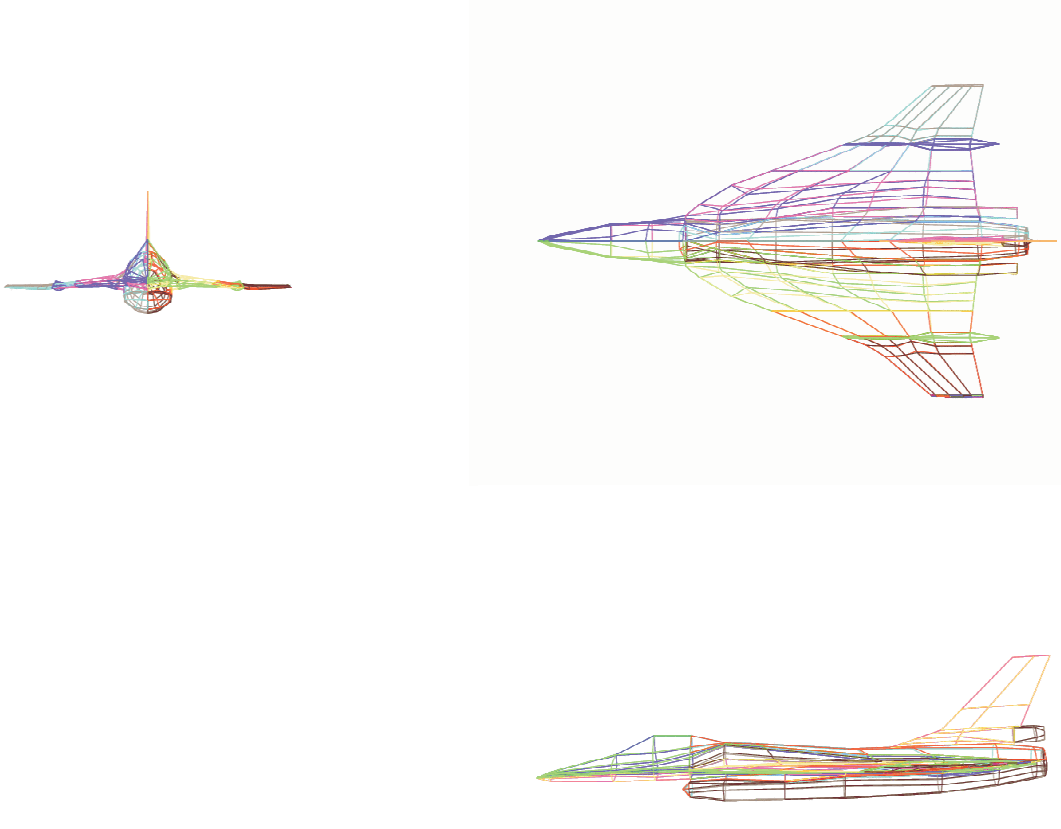

Figure 2. Three-view of F-16XL computational model.

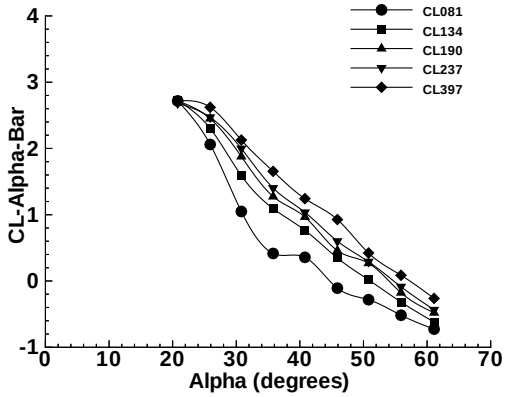

Figure 3. In-phase lumped dynamic lift force coefficient derivative, $\bar{C}_{L_\alpha}$, from Ref. 6.

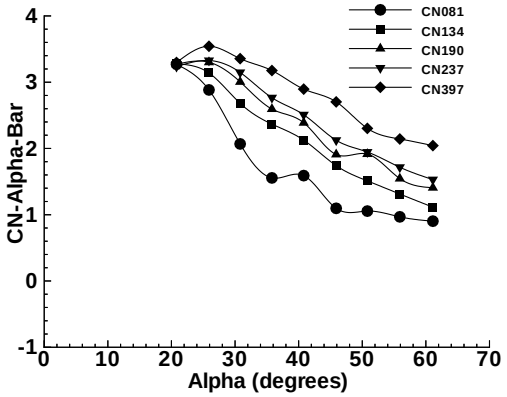

Figure 6. In-phase lumped dynamic normal force coefficient derivative, $\bar{C}_{N_\alpha}$, from Ref. 6.

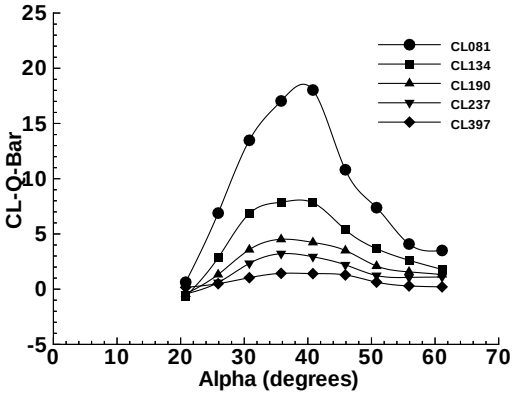

Figure 4. Out-of-phase lumped dynamic lift force coefficient derivative, $\bar{C}_{L_q}$, from Ref. 6.

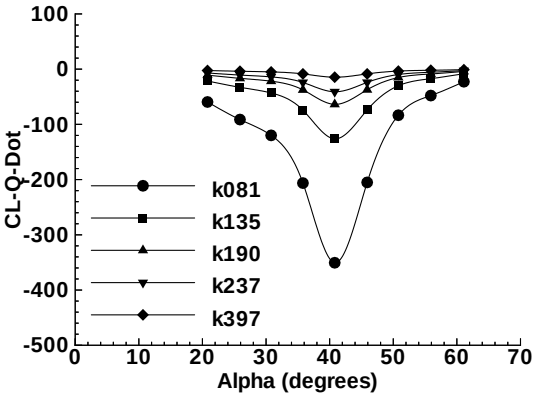

Figure 7. Derived lift force coefficient derivative data, $C_{L_{\dot{q}}}$.

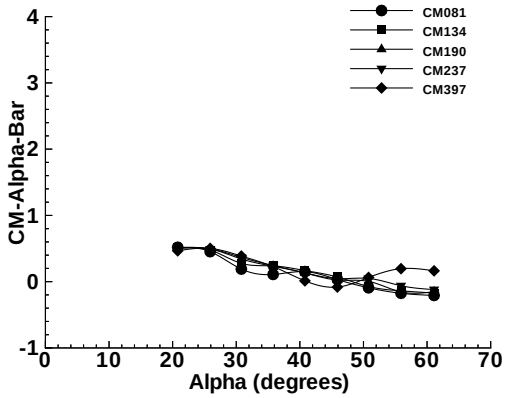

Figure 5. In-phase lumped dynamic pitching moment coefficient derivative, $\bar{C}_{M_\alpha}$, from Ref. 6.

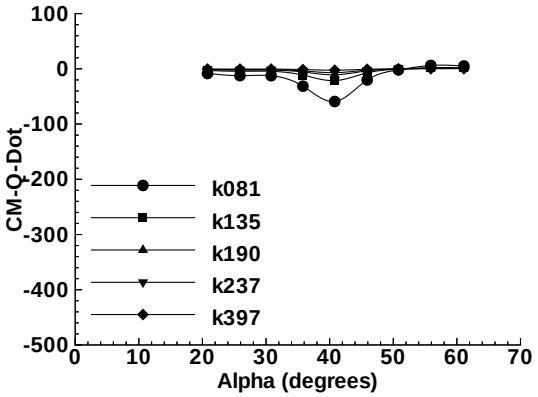

Figure 8. Derived pitching moment coefficient derivative data, $C_{M_{\dot{q}}}$.

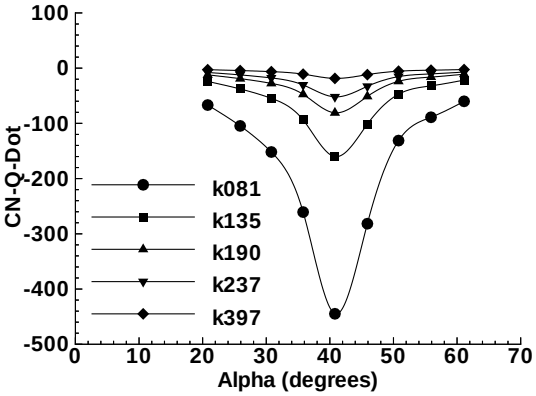

Figure 9. Derived normal force coefficient derivative data, $C_{N_{\dot{q}}}$.

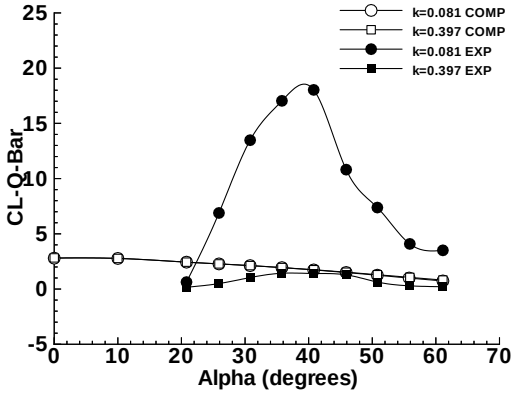

Figure 11. Out-of-phase lumped computed and measured dynamic lift force coefficient derivative, $\bar{C}_{L_q}$.

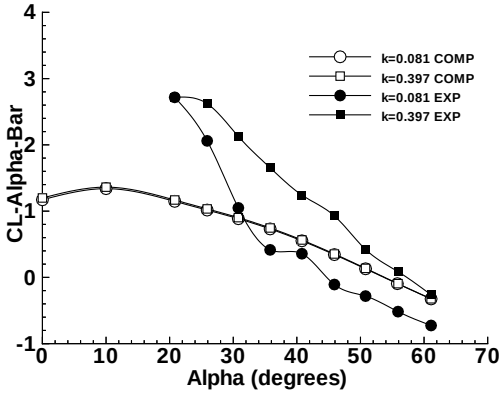

Figure 10. In-phase lumped computed and measured dynamic lift force coefficient derivative, $\bar{C}_{L_\alpha}$.

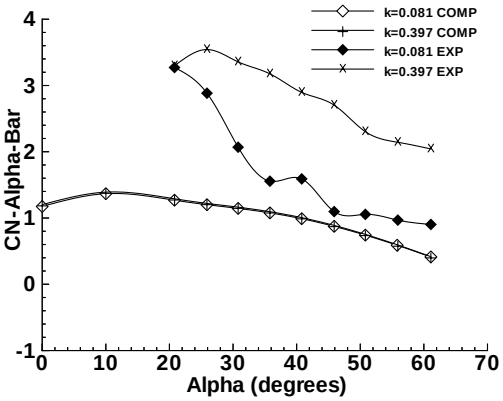

Figure 12. In-phase lumped computed and measured dynamic normal force coefficient derivative, $\bar{C}_{N_\alpha}$.

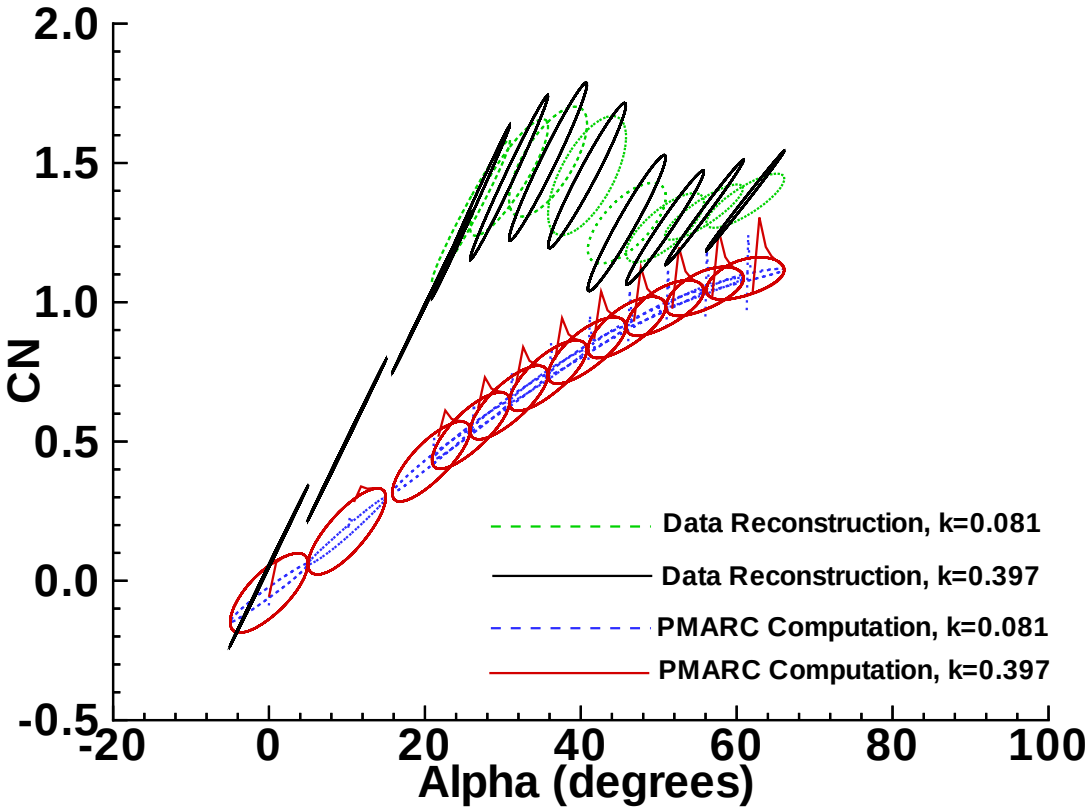

Figure 13. Computed and reconstructed normal force coefficient data.